Pergamon

Int. J. Solids Structures Vol. 34, No. 23, pp. 2969–2990, 1997

0020–7683/97 $17.00 + .00

PII: S0020–7683(96)00220–X

SIMPLIFIED ANALYTICAL MODELS FOR TRANSIENT UNIAXIAL WAVES IN A LAYERED PERIODIC STACK

MICHAEL EL-RAHEB
Dow Chemical Company, Central Research, Building 1776, Midland, MI 48674, U.S.A.

(*Received* 25 *January* 1996; *in revised form* 10 *October* 1996)

Abstract—A physical understanding is gained of some results acquired in the analysis of transient propagation of uniaxial elastic waves in weakly coupled periodic stacks using simple analytical models. Three simplified models are examined: a mass–spring chain, a single mass spring attached to a delayed moving base, and high frequencies of an elastic mass reacted upon by a spring. Closed-form expressions and asymptotic behavior are obtained for attenuation of maximum stress, characteristic velocities, internal stress distribution and transmission or suppression of high-frequency oscillations. The results provide insights in the design of impact resistant structural systems using layered periodic stacks. © 1997 Elsevier Science Ltd.

1. INTRODUCTION

The study of transient uniaxial waves in layered media is useful in composites, geophysics, ocean acoustics and oil exploration. A large body of work was produced that treated the harmonic propagation of waves in layered media excited by monochromatic sources. Thompson (1950), Haskel (1953), Rytov (1956), Anderson (1961) and Tennenbaum (1992) discussed time harmonic propagation in 1-D layered media. Sun (1968), Delph (1978, 1979, 1980), and Herrmann (1982) extended the time periodic waves to 3-D periodic media. Mead (1971, 1975, 1978, 1984, 1986), Engels (1978), Gupta (1980), McDaniel (1982), Faulkner (1985), Keane (1989) and Rousseau (1989) considered simple periodic structures and applied Floquet theory to propagation and attenuation zones. Robinson (1972), Lee (1973), Chao (1975), Golebiewska (1980), Shah (1982), Kundu (1985), Mal (1988), and Braga (1990) discussed waves in composites. The methods used to analyze this problem ranged from purely numerical, like discretization and geometric optics, to purely analytical, like modal and transform techniques. In contrast with the extensive work reported on harmonic waves, little attention was devoted to transient waves despite their importance in many practical applications. El-Raheb (1993) treated transient uniaxial waves in finite ordered and disordered bi-periodic stacks. The method relied on deriving transfer matrices in harmonic space relating state vectors at the interface between layers. Equilibrium of stress and continuity of displacement at each interface produced a system of tri-diagonal block matrices yielding the modal characteristics of the stack. Transient response was found from an expansion in these modes. Clearly, the complexity of the analytical solution in El-Raheb (1993) limits its usefulness in developing insights into the character of uniaxial propagation. In this reference, results on transient uniaxial waves were obtained for a stack of alternating hard and weak layers excited by a trapezoidal pulse of short duration (see Fig. 1(a)).

The purpose of this study is to gain physical understanding of these results by a series of less general but simpler consistent analytical models, from which concise formulae describing propagation can be obtained. These models include: (A) the lumped mass–spring model; (B) the oscillator with delayed moving boundary model; and (C), the high frequency transmission model. A complete account of each model is found in the Appendices.

Since the first propagation zone (PZ1) of the weakly coupled periodic stack is paramount in propagation, the first simplified Model (A) termed "lumped mass–spring chain"

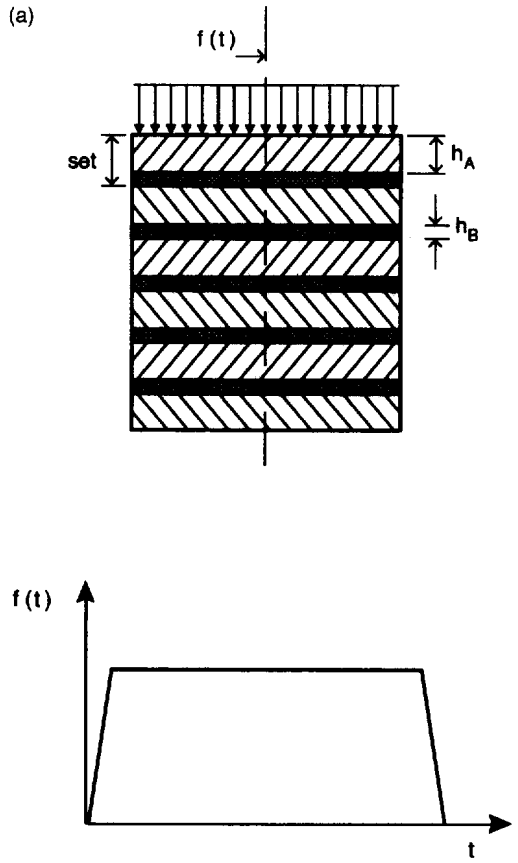

Fig. 1. (a) Geometry of periodic stack and trapezoidal forcing pulse. (b) Histories of u (microns) and σ at interface of sets along the basic stack with $m_s = 20$, $\mathscr{S} = 1.034$, trapezoidal pulse with $t_f = 20$ μs. (*Continued opposite.*)

reduces the continuum to a finite number of identical masses connected by weak springs where each hard layer acts as rigid mass and each weak layer acts as a massless spring. Results from this model re-confirm the importance of PZ1 on transient response and yield simple expressions for phase and group velocities c_p and c_g in PZ1 in terms of properties of hard and weak layers. Furthermore, an integral of the dynamic equations of motion of each set yields a conservation law relating maximum stress of first arrival to width of the trapezoidal forcing pulse and period of the primary stress wave prior to reflections. Indeed, this is identical to the scaling law derived in El-Raheb (1993) relating peak stress of first arrival to frequency interval of PZ1 and width of the trapezoidal forcing pulse. Model (A) also explains distribution of peak stress of first arrival within a hard layer and location of its minimum along the layer.

The almost exact match of response histories from Model (A) and the modal solution in El-Raheb (1993) suggests one more level of simplification and Model (B) termed "the delayed moving boundary", which confines itself to a single mass and a single spring of Model (A) but with the spring connected to a base duplicating a delayed motion of the mass (see Fig. 10(a)). The hypothesis behind this model is that the wave front moves along the stack at the transient phase velocity in PZ1. This means that a pulse produced on top of a set arrives at the interface between one set and the adjacent set after a time delay equaling the thickness of the periodic set divided by transient phase velocity. Since the phase velocity derived in Model (A) is frequency dependent and the resonant frequency of a mass–spring set is the dominant frequency in the dispersed pulse, phase velocity is then evaluated at that frequency, which equals half the frequency interval in PZ1. Results of this model agree closely with results of Model (A). In this way, propagation in a weakly coupled periodic stack is reduced to its simplest constituents, namely frequency of the set and phase

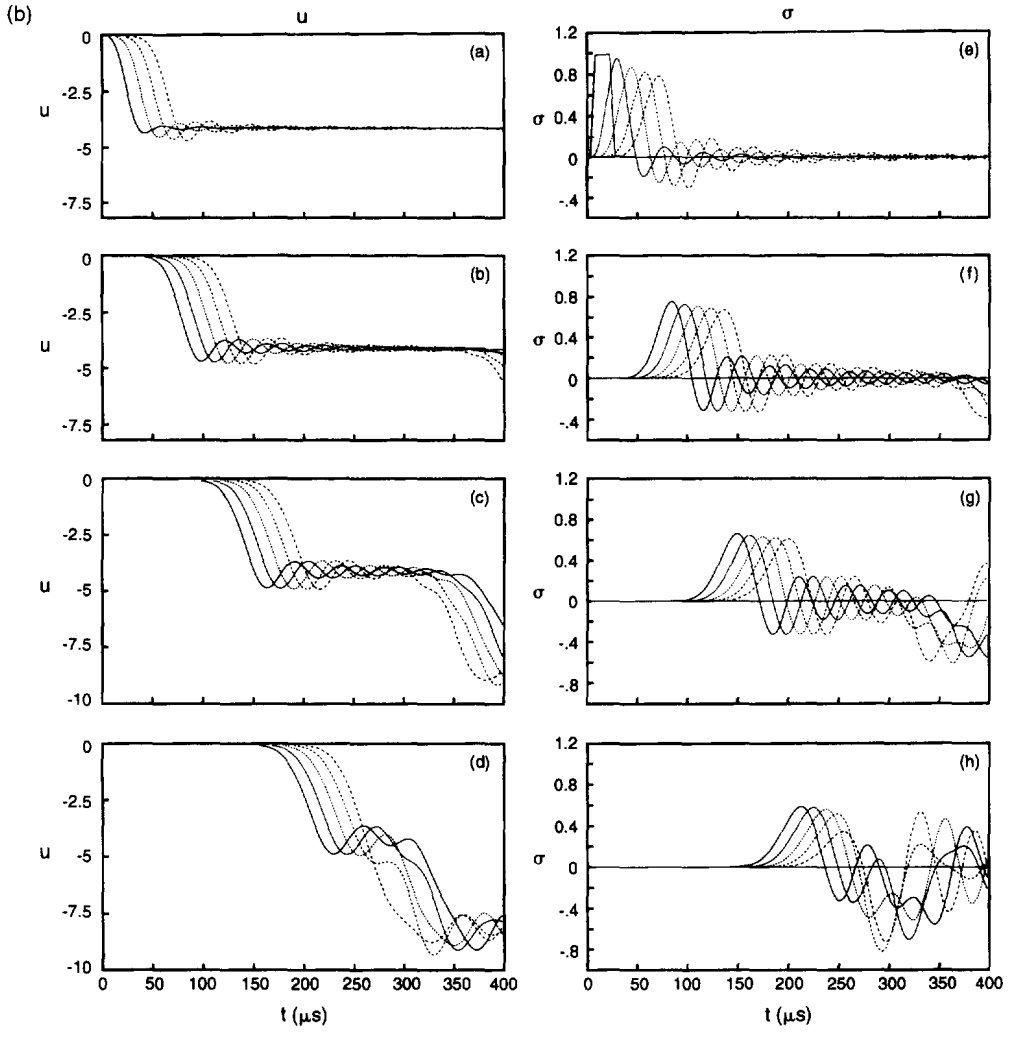

Fig. 1—*Continued.*

velocity evaluated at that frequency. This Model also shows that rate of attenuation of peak stress of first arrival along the stack is proportional to arrival time to the power $-1/3$.

As explained in El-Raheb (1993), the second propagation zone PZ2 modulates response by high frequency from elastic resonances of the hard layer. The third Model (C), termed "transmission of elastic frequencies of the hard layer", relies on analysis of a single set including elasticity of the hard layer. It identifies the two parameters controlling high frequency transmission as rise time of the forcing pulse and dynamic stiffness of the periodic set. Furthermore, a simplified expression for stress response shows that if the period of elastic resonance of the hard layer equals rise time of the forcing pulse, high frequency is suppressed.

Section 2 reviews results of El-Raheb (1993) and summarizes important features of transient uniaxial propagation in a finite periodic stack. Section 3 derives Model A of the finite lumped mass–spring chain. Section 4 derives Model B. Section 5 derives Model C.

2. REVIEW OF RESULTS IN EL-RAHEB (1993)

The following lists results in El-Raheb (1993), each accompanied by a brief explanation or extension obtained by the present analysis:

1. In weakly coupled bi-periodic uniaxial stacks (see Fig. 1(a)), frequency response is divided into propagation zones PZ and attenuation zones AZ similar to pass and stop

bands in a filter. It was observed that the first propagation zone PZ1 is paramount. In fact, motions in PZ1 are those of a finite rigid mass–spring chain.

2. At a fixed point along the stack, peak stress response prior to reflections from an external boundary is termed peak stress of first arrival, σ^1_{mx}. In El-Raheb (1993), a non-dimensional parameter, transmissibility $\mathscr{I}$, was derived that scales and controls σ^1_{mx}. Wave transmissibility is defined as $\mathscr{I} = \Delta\omega_{PZ1} t_f/\pi$ where $\Delta\omega_{PZ1}$ is the frequency interval of PZ1 and t_f is the time interval of the equivalent rectangular forcing function that conserves impulse. In a stack of bi-periodic sets made of two materials A and B, $\Delta\omega_{PZ1} \simeq 2c_A/[h_A(\tilde{z}\tilde{\tau})^{1/2}]$ where $c_{A,B}$ is the speed of sound, $\rho_{A,B}$ is density, $h_{A,B}$ is thickness in layers A and B, $\tilde{z} = (\rho_A c_A)/(\rho_B c_B)$ is ratio of acoustic impedances, and $\tilde{\tau} = (h_B c_A)/(h_A c_B)$ is ratio of travel times. When $\mathscr{I} < 1$, σ^1_{mx} is attenuated, while when $\mathscr{I} > 1$, σ^1_{mx} is initially magnified, reaching a maximum and then attenuating along the stack. These results, as well as a relation between σ^1_{mx} and $\mathscr{I}$ are obtained by the mass–spring chain description in a conservation form.
3. In the hard layer, σ^1_{mx} is larger at the interfaces than within. A caustic generated by the envelope of the instantaneous linear stress distributions is obtained based on the mass–spring chain description that shows a minimum of σ^1_{mx} occuring at $0.6h_A$.
4. An expression was obtained for maximum phase velocity c_0 in the limit when frequency ω is zero. This expression is extended using the mass–spring chain description to a Taylor's series expansion of both phase velocity c_p and group velocity c_g in terms only of even powers of the frequency parameter $(\omega h_s/c_0)$ where $h_s = h_A + h_B$ is the thickness of a periodic set. The ratios c_p/c_0 and c_g/c_0 are insensitive to $\mathscr{I}$.
5. When σ^1_{mx} attenuates along the stack, it does so monotonically. The asymptotic behavior of σ^1_{mx} in terms of arrival time of the wave front t_p is obtained by the delayed moving base model.
6. High frequency oscillations H.F. are enhanced or suppressed depending on stack configuration. By treating the hard layer as an elastic body reacted by the spring of the weak layer, an expression for H.F. response is derived in terms of the fundamental elastic resonant frequency of the hard layer and rise time of the forcing pulse. Also derived is an expression for dynamic stiffness which controls H.F. amplitude.

In the sections to follow, the observations listed above will be tested, explained or expanded upon following the same order as the introduction. Unless otherwise indicated, the same test case will be used in examining the simplified models as in El-Raheb (1993). By generating and displaying again the results of El-Raheb (1993) as well as results of the simplified models, it is assured that they faithfully reproduce the observation to be explained.

From El-Raheb (1993), the properties of the basic stack (see Fig. 1(a)) with 20 biperiodic sets ($m_s = 20$) are:

$$h_A = 1.245\,\text{cm}; \quad h_B = 0.025\,\text{cm}$$
$$E_A = 320\,\text{GPa}; \quad E_B = 69\,\text{MPa}$$
$$\rho_A = 3.25\,\text{g/cm}^3; \quad \rho_B = 1.07\,\text{g/cm}^3.$$

The trapezoidal forcing function is of unit intensity, with 5 μs rise and fall times, and a 15 μs plateau (see Fig. 1(a)). The highest propagation zone in the modal expansion includes the second elastic resonance of the hard layer. For the basic stack this translates to a frequency of 800 kHz.

3. LUMPED MASS–SPRING CHAIN

In Fig. 1(b) there appears histories of displacement u and stress σ at the interfaces between layers in the stack. Each box groups histories at five consecutive interfaces. At each interface, u rises smoothly reaching a plateau after the forcing function elapses. The plateau is disrupted by the reflected wave from the farthest set, $n = 20$. The behavior of succeeding sets is shifted in time by an interval $t_d^{(n)} = nh_s/c_p$ where n is set number. These

states of motion are typical of transient waves of rigid masses coupled by weak springs, showing that the response is largely determined by PZ1 (see Appendix A). The results from the method in El-Raheb (1993) and Model A are indistinguishable in this figure, which confirms the adequacy of restricting the continuum model to PZ1. The effects of dispersion, namely attenuation in σ^1_{mx} and growth in trailing oscillations are clear from Fig. 1(b), graphs (e)–(h). As the wave front moves further into the stack, $\partial\sigma/\partial t$ decreases, the pulse becomes wider, and σ^1_{mx} attenuates to conserve linear momentum.

In Appendix A, the mass–spring chain description is developed. With the hypothesis that prior to reflection from an external boundary, displacement histories at interfaces of a layer tend to quiescence, the following form of conservation of momentum is derived:

$$\int_0^{t_L} \sigma_1 \, dt = I_p$$

$$\int_0^{t_L} \sigma_i \, dt = \int_0^{t_L} \sigma_{i-1} \, dt = I_p \tag{A14}$$

where σ_i is stress in the ith spring, t_L is time for quiescence and I_p is impulse. Furthermore, approximating the shape of the dispersed stress wave at the first interface by

$$\sigma_1(t) \simeq \frac{1}{2}\sigma^1_{mx}\left[1-\cos\left(2\pi\frac{t}{T}\right)\right], \quad t \leqslant T \tag{1}$$

where T is the period of the primary wave, and substituting (1) in (A14) with $t_L = T$ yields

$$\sigma^1_{mx}\frac{T}{2} = \sigma_0 t_f = I_p$$

$$\Rightarrow \tilde{\sigma}^1_{mx} \equiv \sigma^1_{mx}/\sigma_0 = 2t_f/T \tag{2}$$

where t_f is the width of the equivalent rectangular forcing pulse delivering I_p. The period T of the primary stress wave depends on the relative magnitude of $2t_f$ and π/ω_e where ω_e is the resonant frequency of the mass–spring set:

$$T \cong \max\left[2t_f, \pi/\omega_e\right] \tag{3}$$

when $2t_f \leqslant \pi/\omega_e$, $\tilde{\sigma}^1_{mx} \simeq 2\omega_e t_f/\pi = \mathscr{I}$. When $t_f > \pi/\omega_e$, $\tilde{\sigma}^1_{mx} \cong 1$. Therefore, if $\mathscr{I} < 1$, $\tilde{\sigma}^1_{mx} < 1$, and only if $\mathscr{I} > 1$ can $\tilde{\sigma}^1_{mx}$ exceed unity, which was the conclusion also reached in El-Raheb (1993).

In Fig. 2 there appears histories of σ for the basic stack along the first three hard layers. Histories at six equidistant stations in each layer including the interfaces are grouped. Figure 2(a) shows how σ evolves along the first layer from the trapezoidal shape at the excited face, to the dispersed shape at the interface with the weak layer. In each of the following hard layers (see Fig. 2(b), (c)) histories at the different stations in a layer cross at the point where σ^1_{mx} is minimum. This fact, not obvious before the results were obtained and plotted, requires explanation. Consider the distribution of modal stress in a hard layer given by the transfer matrix in eqn (2) of El-Raheb (1993):

$$u_x = \cos(k_A x)u_L + (1/k_A E_A)\sin(k_A x)\sigma_L \tag{4a}$$

$$\sigma_x = -k_A E_A \sin(k_A x)u_L + \cos(k_A x)\sigma_L \tag{4b}$$

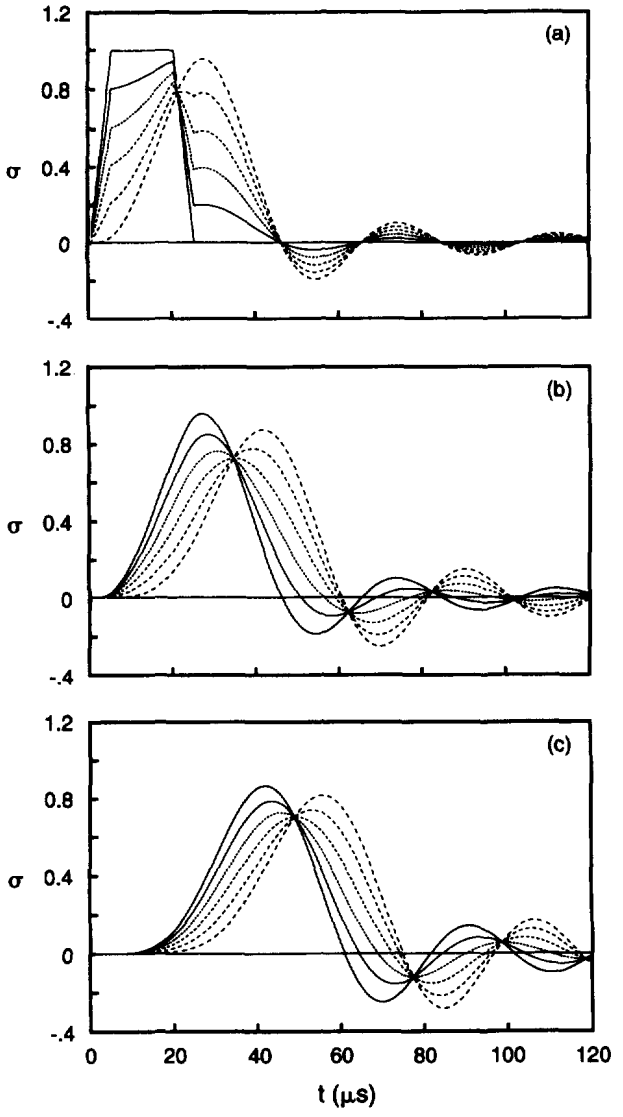

Fig. 2. Histories of σ within each of the first 3 sets of the basic stack with $m_s = 20$, $\mathscr{I} = 1.034$, $t_f = 20$ μs.

where subscripts L and x denote quantities at the left boundary and at station x along the layer, and $k_A = \omega/c_A$. For modes in PZ1 :

$$k_A x \leqslant \frac{\Delta\omega_{\mathrm{PZ1}} x}{c_A} \simeq \frac{2x}{h_A}(\tilde{z}\tilde{t})^{-1/2} < 0(1). \tag{5}$$

Expanding $\sin(k_A x)$ and $\cos(k_A x)$ in (4b) for small $(k_A x)$ yields

$$\sigma_x \cong -\omega^2 \rho_A u_L x + \sigma_L. \tag{6}$$

Equation (6) shows that in PZ1, modal stress is linear with x. Since transient stress is the superposition of modal stresses, it too is linear with x.

Figure 3(a)–(d) traces the time evolution of σ within one particular hard layer. Each line corresponds to a σ distribution at some fixed time t. The caustic generated by the envelope of these lines coincides with σ^1_{mx}. The results are shown for four different stacks within the range of $0.478 \leqslant \mathscr{I} \leqslant 1.551$. It is clear in every case that σ^1_{mx} is minimum at $x/h_A = 0.6$. From Fig. 4 showing caustics in the three hard layers following the first for

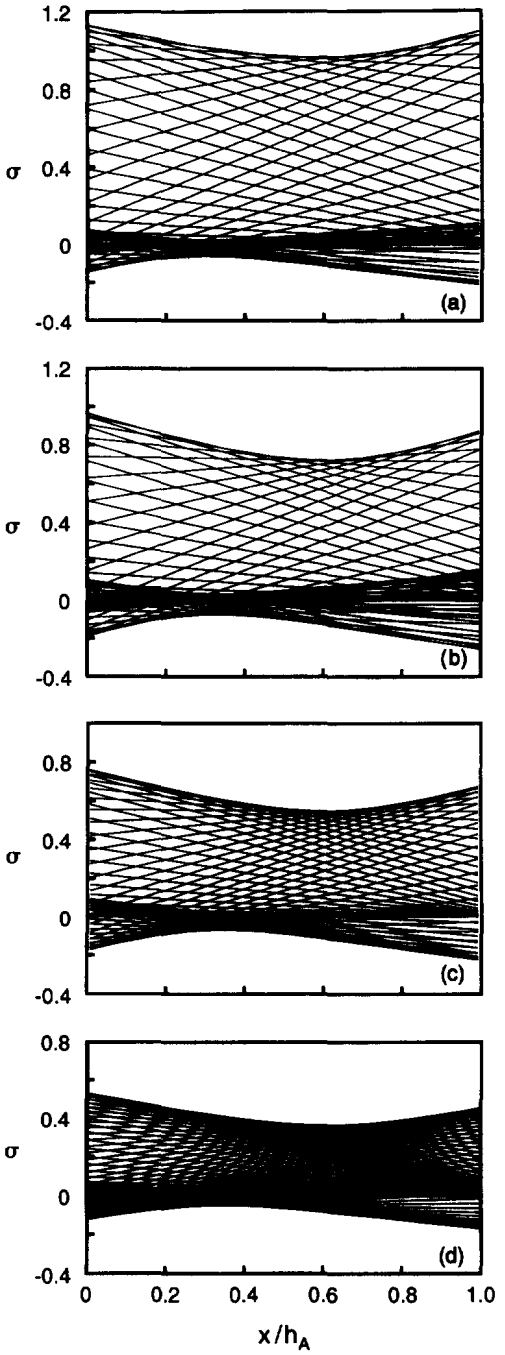

Fig. 3. Distribution of a σ along 2nd hard layer with t as parameter and formation of caustic (a) $\mathscr{F} = 1.551$, (b) $\mathscr{F} = 1.034$, (c) $\mathscr{F} = 0.738$, (d) $\mathscr{F} = 0.478$.

each of the four values of $\mathscr{F}$, it becomes clear that this is true also independent of $\tilde{z}$, $\tilde{\tau}$ and t_f.

The parametric equation of the caustic may be determined from (6) using

$$\sigma(x,t) = (\sigma_R(t) - \sigma_L(t))\frac{x}{h_A} + \sigma_L(t) \tag{7}$$

where subscripts L and R denote quantities at left and right of a layer. If $x_c(t)$ is the local

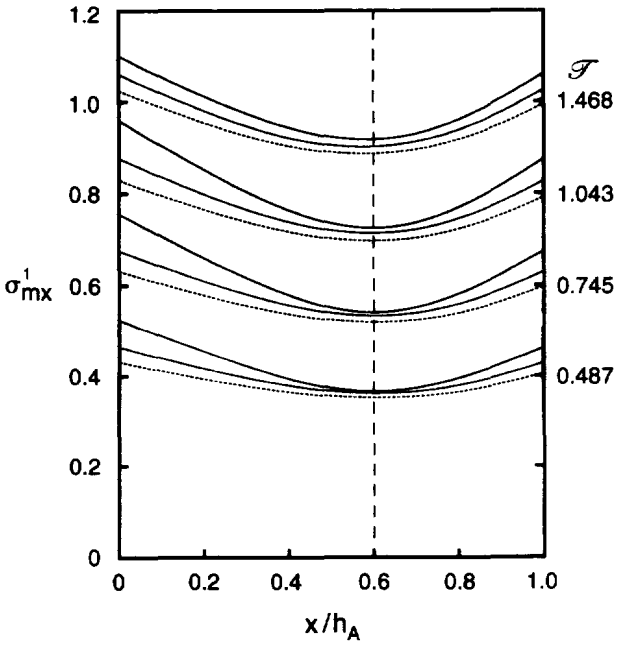

Fig. 4. Distribution of peak stress of first arrival σ^1_{mx} within sets 2 —, 3 ···, 4 --- for different $\mathscr{F}$ values.

axial coordinate at a point on the caustic, holding x fixed, then finding the extrema of the function in (7) yields $(x_c, \sigma_c(x_c))$:

$$\frac{x_c}{h_A} = -\frac{\dot{\sigma}_L}{(\dot{\sigma}_R - \dot{\sigma}_L)} \tag{8}$$

where $(\dot{})$ is time derivative. Substituting (8) in (7) gives σ_c at x_c:

$$\sigma_c = -\frac{(\sigma_R - \sigma_L)}{(\dot{\sigma}_R - \dot{\sigma}_L)}\dot{\sigma}_L + \sigma_L = \sigma^1_{mx}(t). \tag{9}$$

Then σ_c is an extremum at the x_c where

$$\frac{\partial \sigma_c}{\partial x_c} = 0 \Rightarrow \frac{\dot{\sigma}}{\dot{x}_c} \equiv \frac{\sigma_R - \sigma_L}{h_A} = 0. \tag{10}$$

Clearly, the minimum occurs at some $t = t_{mn}$ when $\sigma_R(t_{mn}) = \sigma_L(t_{mn})$

$$\sigma_{cmn} = \sigma_L(t_{mn}) = \sigma_R(t_{mn})$$
$$\frac{x_{cmn}}{h_A} = -\frac{\dot{\sigma}_L}{(\dot{\sigma}_R - \dot{\sigma}_L)}\bigg|_{t=t_{mn}}. \tag{11a}$$

This implies that σ^1_{mx} achieves a minimum within a hard layer when stress is uniform throughout that layer, and confirms that all stress histories cross at t_{mn}. That $x_{cmn}/h_A = 0.6$ implies that instantaneously at $t = t_{mn}$, the σ line rotates about x_{cmn} yielding

$$\dot{\sigma}_R(t_{mn}) = -\tfrac{2}{3}\dot{\sigma}_L(t_{mn}). \tag{11b}$$

From eqn (20) in El-Raheb (1993), the exact expression for propagation constant μ is:

$$\cos\mu = -\frac{1+\tilde{z}^2}{2\tilde{z}}\sin\gamma\sin(\gamma\tilde{\tau})+\cos\gamma\cos(\gamma\tilde{\tau}) \equiv \Gamma \tag{12}$$

where $\gamma = \omega h_A/c_A$. By definition

$$c_p = \frac{\omega}{k} = \frac{\omega h_s}{\mu} = \frac{\omega h_s}{\cos^{-1}(\Gamma)} \tag{13}$$

$$c_g = \frac{\partial\omega}{\partial k} = \frac{h_s c_A}{h_A}\sin\mu\left\{\frac{1+\tilde{z}^2}{2\tilde{z}}[\cos\gamma\sin(\gamma\tilde{\tau})+\tilde{\tau}\sin\gamma\cos(\gamma\tilde{\tau})]\right.$$
$$\left.+\sin\gamma\cos(\gamma\tilde{\tau})+\tilde{\tau}\cos\gamma\sin(\gamma\tilde{\tau})\right\}^{-1}. \tag{14}$$

In PZ1, $\gamma \leqslant 2(\tilde{z}\tilde{\tau})^{-1/2} < 0(1)$. Expanding (12) for small γ then substituting in (13) and (14) yields

$$c_p \simeq c_0[1-v_2\gamma_p^2-v_4\gamma_p^4+0(\gamma_p^6)] \tag{15a}$$

$$c_g \simeq c_0[1-3v_2\gamma_p^2-3v_4\gamma_p^4+0(\gamma_p^6)] \tag{15b}$$

where

$$\gamma_p = \frac{\omega h_s}{c_0} = \frac{\omega}{\omega_e} = \frac{2\omega}{\Delta\omega_{PZ1}} = 2\tilde{\omega}, \quad c_0 = c_A\frac{h_s}{h_A}\left[\tilde{\tau}\frac{1+\tilde{z}^2}{\tilde{z}}+1+\tilde{\tau}^2\right]^{-1/2}$$

$$v_2 = [-2(1+\tilde{\tau}^2)+\tilde{\tau}\tilde{z}]/(24\tilde{\tau}\tilde{z})$$

$$v_4 = [17(\tilde{\tau}\tilde{z})^2-20(\tilde{\tau}\tilde{z}+3)(1+\tilde{\tau}^2)-120\tilde{\tau}^2]/5760(\tilde{\tau}\tilde{z})^2.$$

For $\tilde{\tau} = 0(1)$ and large $(\tilde{\tau}\tilde{z})$: $v_2 \simeq 1/24$, $v_4 \simeq 17/5760$. These values duplicate results in Balanis (1975). From (15a, b) it follows that:

$$c_p > c_g$$

$$c_p - c_g \simeq 2v_2 c_0\gamma_p^2+0(\gamma_p^4).$$

This difference between c_p and c_g is responsible for spreading of the pulse since the wave front moves at c_p and σ_{mx}^1 moves at c_g.

The asymptotic expansions (15a, b) motivate using exact expressions for c_p and c_g in plots of (c_p/c_0) and (c_g/c_0) against γ_p, as shown in Fig. (5a), where the range $0 \leqslant \gamma_p \leqslant 2$ is the width of PZ1. Figure 5(b) plots the same quantities against (h_s/λ) where $\lambda = 2\pi/k$ is wave length. The curves in Fig. 5 are indistinguishable for different $\tilde{\tau}$ and $\tilde{z}$ in the range $0.4 \leqslant \mathscr{S} \leqslant 1.5$.

4. OSCILLATOR WITH DELAYED MOVING BOUNDARY

The simplest adequate model will describe how σ_{mx}^1 varies along the stack. It is built in two steps: first, deriving expressions for stress at the first interface; second, determining how σ_{mx}^1 attenuates in following layers. Recall how the displacement history in Fig. 1(b), graph (a) led to the lumped Model A. Motion of the first layer can be approximated by that of single mass–spring oscillator with mass driven by the external force and spring

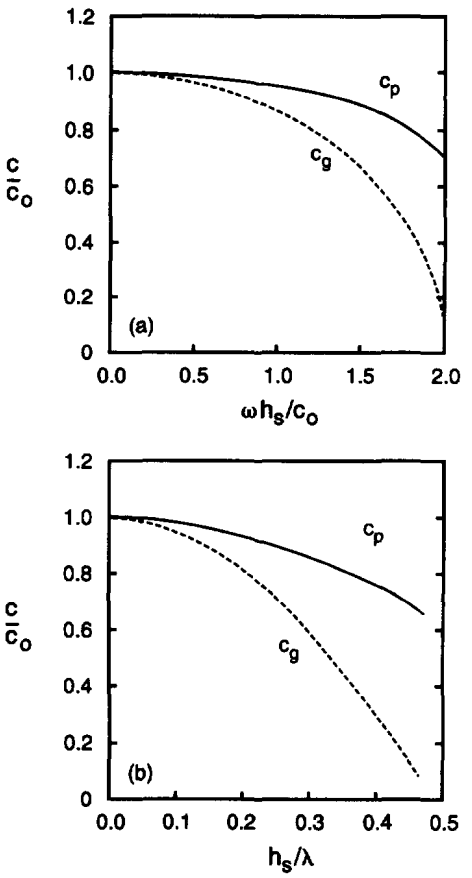

Fig. 5. Phase velocity c_p (—), and group velocity c_g (- - -), in the first propagation zone.

connected to a moving base. The base displacement is the same as the mass but with a time delay $t_d = c_p(\omega_e)/h_s$ where $c_p(\omega_e)$ is phase velocity evaluated at the frequency of the lumped model, $\omega_e = \frac{1}{2}\Delta\omega_{PZ1}$. Closed-form expressions for u and σ of this new simpler Model B of the oscillator with moving base are derived in Appendix B. The response of succeeding masses can be found by repeating the steps above except that stress in the preceding spring acts as a forcing function and dispersion causes $c_p(\omega_e)$ to rise smoothly to $c_p(0) = c_0$. Figure 6 compares histories of u and σ as predicted by El-Raheb (1993) and Model B. Also in Appendix B is derived an asymptotic value of 1/3 for the attenuation α where $\sigma^1_{mx} \propto t_p^{-\alpha}$, and that $c_p(\omega_e) \leqslant c_p \leqslant c_0$ and $c_g(\omega_e) \leqslant c_g \leqslant c_0$.

Figure 7(a)–(c) shows how σ^1_{mx}, c_σ/c_0 and attenuation index α vary along a 46-set stack for three values of $\mathscr{I}$, where c_σ is the transient group velocity of σ^1_{mx} using the mass–spring description. From Fig. 7(a, b) and for $m = 2$, $c_\sigma/c_0 \simeq 0.85$ which coincides with c_g/c_0 at $\omega = \omega_e$ (i.e., $\omega_e h_s/c_0 = 1$) in Fig. 5(a) and also from eqns (A8) and (A9) yielding $c_g/c_0 = \sqrt{3}/2 = 0.866$. This implies that $c_\sigma \cong c_g(\omega_e)$ where the force acts and c_σ approaches c_0 smoothly as the stress wave disperses. When $\mathscr{I} \leqslant 1$, $\sigma^1_{mx} < 1$ everywhere and α increases with m in the interval $0.21 < \alpha < 0.32$. Note that the asymptotic value of α determined numerically is indeed 1/3. α falls as $\mathscr{I}$ increases, apparent from Fig. 7(c) for $\mathscr{I} = 1.631$ where $0.15 < \alpha < 0.28$.

5. TRANSMISSION OF ELASTIC FREQUENCIES OF THE HARD LAYER

Appendix C derives relations for u and σ in the first hard layer including its high frequency (H.F.) elastic resonances according to Model C. These high frequencies correspond to elastic motions of the hard layer in PZ2. From (C12), H.F. amplitude is proportional to $(\omega_1 t_1)^{-1}$ where ω_1 is fundamental resonance of the hard layer and t_1 is the

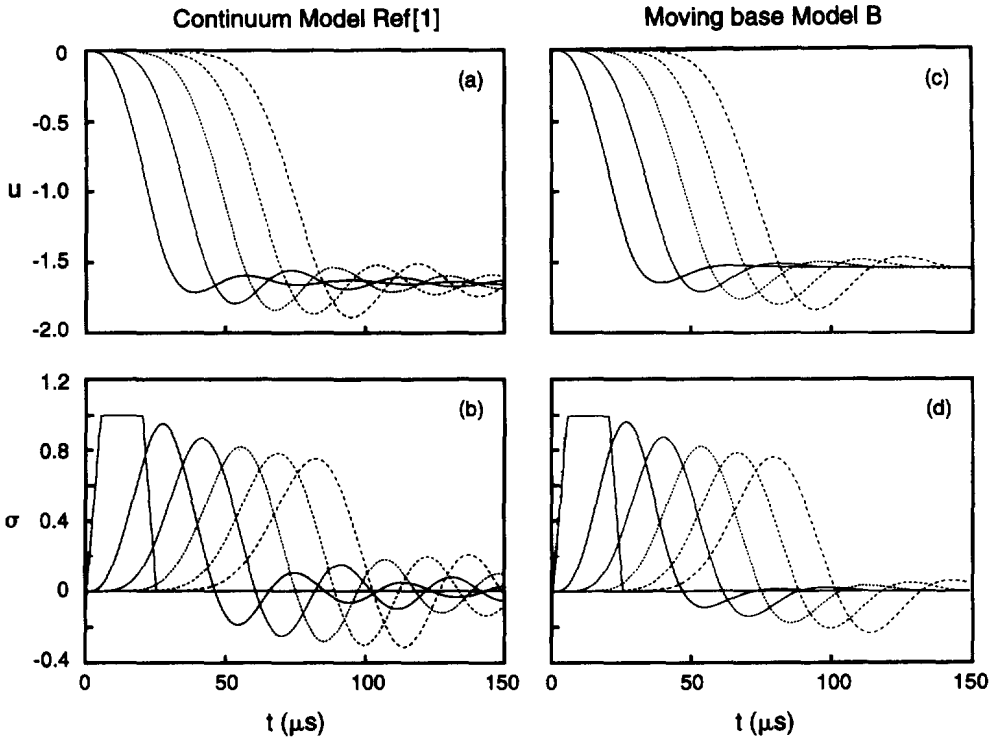

Fig. 6. Histories of u (micro in.) and σ at interface of sets for basic stack with $\mathscr{J} = 1.034$, $t_f = 20$ μs: (a), (b) Continuum Model Ref. [1]; (c), (d) Moving base Model B.

rise time of the trapezoidal pulse. H.F. vanishes if $\omega_1 t_1 = 2j\pi \Rightarrow t_{1s} = j/\Omega_1$. For illustration, return to the case treated in Fig. 2, termed stack I, where $\Omega_1 = 398.2$ kHz and $t_{1s} = j/\Omega_1 = (j)$ 2.5 μs. Clearly, these histories exhibit no H.F. because $t_1 = 5$ μs $= (2) \times 2.5$ μs $= t_{1s}$. Figures 8 and 9 were computed by the method of El-Raheb (1993). In Fig. 8(a)–(f) there appears σ histories in the first two hard layers for $t_1 = 4$ μs, 5 μs and 6 μs. Pulse width has been adjusted to keep t_f at 20 μs. Results for $t_1 = 4$ μs and 6 μs exhibit H.F. The effects are larger for $t_1 = 4$ μs (compare Fig. 8(a) to 8(c)). Figure 8(b), (f) show that H. F. in the second hard layer diminishes. These histories are repeated in Fig. 9(a)–(f) for stack II with $(h_A, h_B) = (0.45, 0.05)$ and unchanged material properties for $t_1 = 3$ μs, 4.6 μs, and 6 μs. For stack II, $\Omega_1 = 433.6$ kHz and $t_{1s} = j/\Omega_1 = (j)$ 2.3 μs. Thus, by the choice $t_1 = 4.6$ μs, the response in Fig. 9(c), (d) becomes free of H.F. Results for $t_1 = 3$ μs and 6 μs exhibit H.F. and the effect is larger for $t_1 = 3$ μs (compare Fig. 9(a) to 9(e)).

Dynamic stiffness of the weak layer determines the nature of transmission of H.F. in hard layers below the first. Except for PZ1, propagation zones belong to one of two types. The first type includes clusters of m_s frequencies centered at a resonance of the unconstrained hard layer $\Omega_{Aj} = jc_A/2h_A$. The second type includes clusters of $(m_s - 1)$ frequencies centered at a resonance of the unconstrained weak layer $\Omega_{Bj} = jc_B/2h_B$. To derive the dynamic spring stiffness k_{Bd} of the weak layer as an extension to Model C by including its inertia, using eqns 4(a), (b), evaluate σ_x, u_x at $x = h_B$, set $u_L = 0$ because the weak layer is assumed fixed to a stationary base as in Model C, and eliminate σ_L:

$$\sigma_x = k_{Bd} u_x$$

$$k_{Bd} = \frac{E_B}{h_B} \gamma_B \cot \gamma_B$$

$$\gamma_B = \frac{2\pi \Omega h_B}{c_B} = \frac{\pi \Omega}{\Omega_{B1}} \tag{16}$$

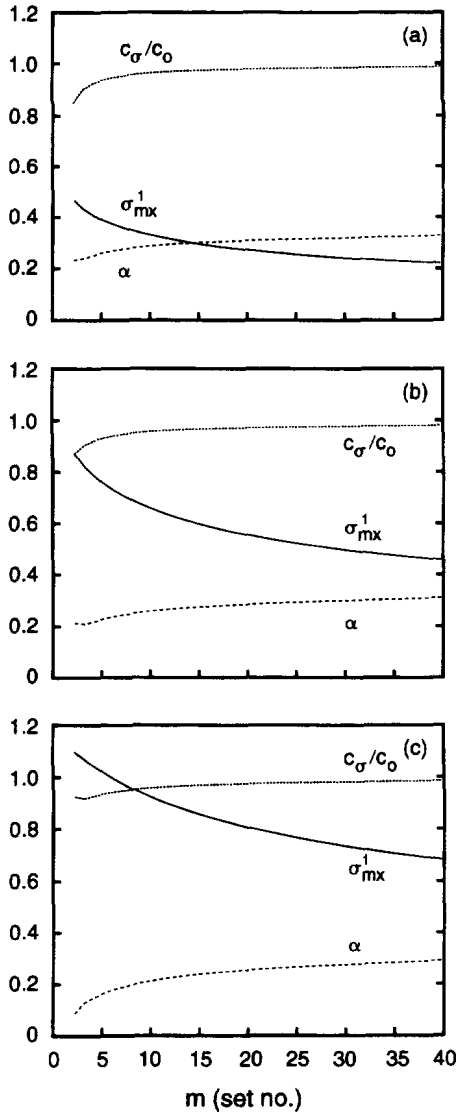

Fig. 7. Variation of σ^1_{mx}, c_σ/c_0 and α along stack with $m_s = 48$, (a) $\mathscr{F} = 0.484$, (b) $\mathscr{F} = 1.040$, (c) $\mathscr{F} = 1.631$.

where Ω is circular frequency of excitation. In PZ1

$$\Omega \ll \Omega_{B1} \Rightarrow \gamma_B \ll 1 \Rightarrow \gamma_B \cot \gamma_B \simeq 1$$
$$\Rightarrow k_{Bd} \simeq E_B/h_B$$

recovering the purely spring stiffness in Model C. In a PZ centered at Ω_{A1}

$$k_{Bd} = \frac{E_B}{h_B}\left(\pi\frac{\Omega_{A1}}{\Omega_{B1}}\right)\cot\left(\pi\frac{\Omega_{A1}}{\Omega_{B1}}\right).$$

As k_{Bd} increases, so does transmission, while amplitude of H.F. diminishes. As k_{Bd} decreases, so does transmission, while amplitude of H.F. intensifies and becomes confined to the first layer. For stack I, $\Omega_{A1} = 398.2$ kHz and $\Omega_{B1} = 500$ kHz producing a $(k_{Bd})_{\mathrm{I}} = 336.3\ E_B$. For stack II, $\Omega_{A1} = 433.6$ kHz and $\Omega_{B1} = 100$ kHz producing a $(k_{Bd})_{\mathrm{II}} = 154.3\ E_B$. Comparing amplitude of H.F. in Fig. 8(a), (b) and Fig. 9(a), (b) shows that stack II is almost twice stack I, consistent with the ratio $(k_{Bd})_{\mathrm{I}}/(k_{Bd})_{\mathrm{II}} \cong 2.2$.

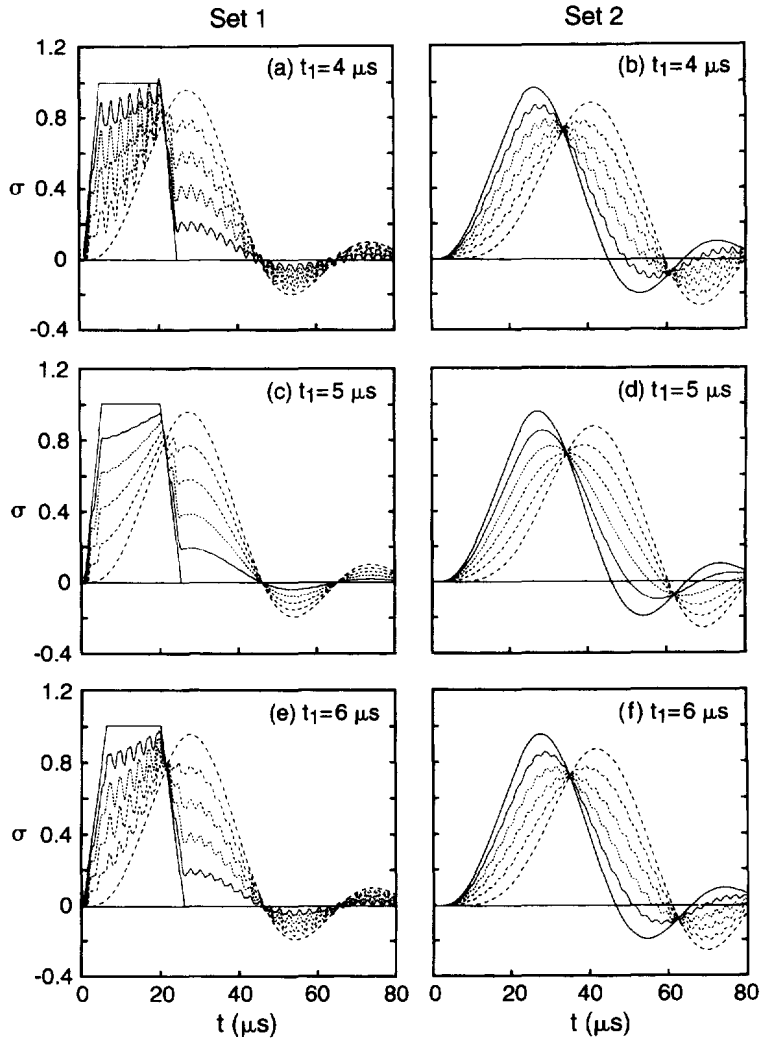

Fig. 8. Histories of σ in the first two sets of stack I with $(h_A, h_B) = (0.49, 0.01)$, $t_f = 20$ μs, $\mathscr{I} = 1.034$: (a), (b) $t_1 = 4$ μs; (c), (d) $t_1 = 5$ μs; (e), (f) $t_1 = 6$ μs.

6. CONCLUSION

Some insights into uniaxial transient waves in weakly coupled periodic stacks are captured by examining a series of simplified analytical models suitably modified to include periodicity and coupling. These models provide accurate description and insights into the mechanics of propagation and interpretation of experimental results. They also provide concise formulas helpful in the design of impact resistant structures by judicious attenuation along the stack of the forcing pulse. Noteworthy results are:

(1) A lumped mass–spring model, Model A, demonstrates that PZ1 dominates response and reduces the governing equations to conservation form. It also establishes transmissibility $\mathscr{I}$ as a scaling parameter.

(2) Model B, a single mass–spring oscillator with delayed moving base, captures the main features of propagation using the dynamic properties of a single set and phase velocity evaluated as its natural frequency, and provides simple expressions for stress at the first interface.

(3) Within a hard layer, peak stress of first arrival σ^1_{mx} achieves a minimum at 0.6 h_A. The phenomenon can be viewed as instantaneous stress lines intersecting to form a caustic surface.

(4) Asymptotic expansions for phase and group velocities c_p and c_g are derived in terms of even powers of frequency parameters $(\omega h_s/c_0)$. The expansions demonstrate that $c_p > c_g$ for all ω in PZ1 and that $(\Delta\omega_{PZ1} h_s)/c_0 \cong 2$. Simpler expressions for c_p and c_g

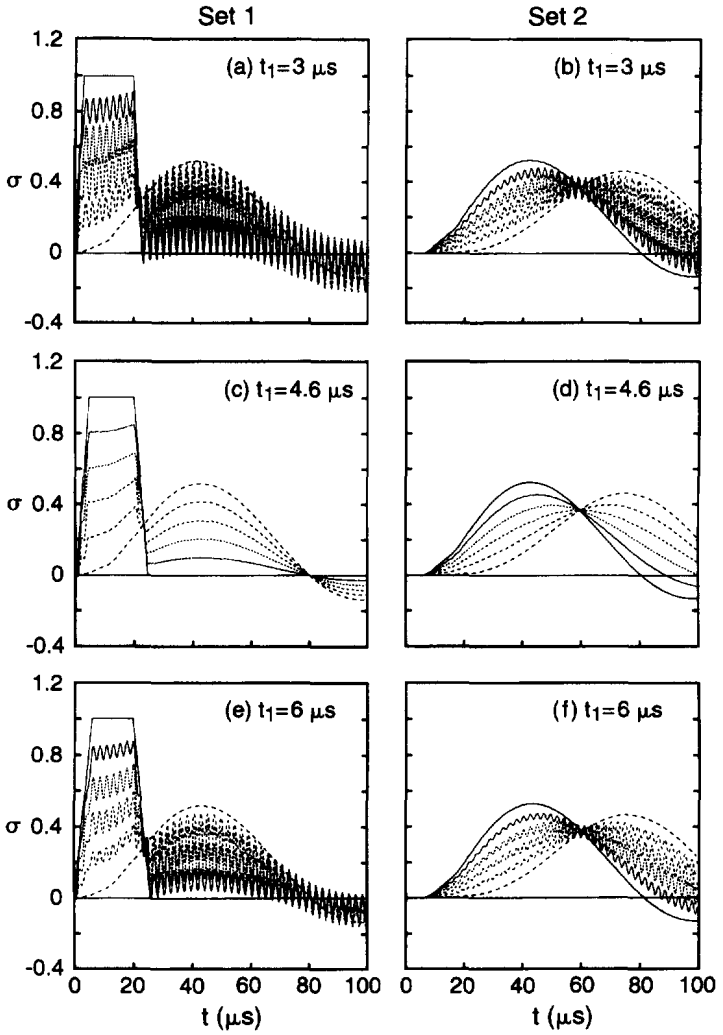

Fig. 9. Histories of σ in the first two sets of stack II with $(h_A, h_B) = (0.45, 0.05)$, $t_f = 20\ \mu s$, $\mathscr{I} = 0.478$: (a), (b) $t_1 = 3\ \mu s$; (c), (d) $t_1 = 4.6\ \mu s$; (e), (f) $t_1 = 6\ \mu s$.

produced by Model A demonstrate that $c_p(\omega_e) \leqslant c_p \leqslant c_0$ and $c_g(\omega_e) \leqslant c_g \leqslant c_0$ where ω_e is frequency of the periodic set.

(5) The attenuation index α, defined by $\sigma^1_{mx} \propto t_p^{-\alpha}$, rises smoothly and slowly along the stack with an asymptote at $\alpha = 1/3$, where t_p is the arrival time of σ^1_{mx}.

(6) Transmission of H.F. into the succeeding hard layers depends on dynamic stiffness of the weak layer k_{Bd} and rise time t_1. Transmission is suppressed for the special cases when $\omega_1 t_1 = 2\pi j$, where ω_1 is elastic axial resonant frequency of the hard layer.

Acknowledgement—The author appreciates Pat Dougherty for her patience and accuracy in typing the manuscript.

REFERENCES

Anderson, D. L. (1961) Elastic wave propagation in layered anisotropic media. *Journal of Geophysical Research* **66,** 2953–2963.

Balanis, G. (1975) Analysis of the dispersion of low frequency uniaxial waves in heterogeneous periodic elastic media. *Journal of Mathematical Physics* **16,** 1383–1387.

Braga, A. M. B. (1990) Wave propagation in anisotropic layered composites. Ph.D. dissertation, Stanford University, Palo Alto, California.

Chao, T. and Lee, P. C. Y. (1975) Discrete-continuum theory for periodically layered composite materials. *Journal of the Acoustical Society of America* **57,** 78–88.

Delph, T. J., Herrmann, G. and Kaul, R. K. (1978) Harmonic wave propagation in a periodically layered infinite elastic body: antiplane strain. *Journal of Applied Mechanics* **45,** 343–349.

Delph, T. J., Herrmann, G. and Kaul, R. K. (1979) Harmonic wave propagation in a periodically layered infinite elastic body: plane strain, analytical results. *Journal of Applied Mechanics* **46,** 113–119.

Delph, T. J., Herrmann, G. and Kaul, R. K. (1980) Harmonic wave propagation in a periodically layered infinite elastic body: plane strain, numerical results. *Journal of Applied Mechanics* **47,** 531–537.
El-Raheb, M. (1993) Transient elastic waves in finite layered media: One-dimensional analysis. *Journal of the Acoustical Society of America* **94,** 172–184.
Engels, R. C. and Meirovitch, L. (1978) Response of periodic structures by modal analysis. *Journal of Sound and Vibration* **56,** 481–493.
Faulkner, M. G. and Hong, D. P. (1985) Free vibrations of a mon-coupled periodic systems. *Journal of Sound and Vibration* **99,** 29–42.
Golebiewska, A. A. (1980) On dispersion of periodically layered composites in plane strain. *Journal of Applied Mechanics* **47,** 206–207.
Gradshteyn, I. and Ryzhik, I. (1970) *Table of Integrals, Series and Products.* Academic Press, New York.
Gupta, Sen G. (1980) Vibration of periodic structures. *The Shock and Vibration Digest* **12**(3), 17–29.
Haskel, N. A. (1953) The dispersion of surfaced waves in multi-layered media. *Bulletin of the Seismic Society of America* **43,** 17–34.
Herrmann, G. and Hemami, M. (1982) Plane-strain surface waves in a laminated composite. *Journal of Applied Mechanics* **49,** 747–753.
Keane, A. J. and Price, W. G. (1989) On the vibrations of mono-coupled periodic and near-periodic structures. *Journal of Sound and Vibration* **128,** 423–450.
Kundu, T. and Mal, A. K. (1985) Elastic waves in a multilayered solid due to a dislocation source. *Wave Motion* **7,** 459–471.
Lee, E. H. and Yang, W. H. (1973) On waves in composite materials with periodic structure. *SIAM Journal of Applied Mathematics* **25,** 492–488.
Mal, A. K. (1988) Wave propagation in layered composite laminates under periodic surface loads. *Wave Motion* **10,** 257–266.
McDaniel, T. J. and Carroll, M. J. (1982) Dynamics of biperiodic structures. *Journal of Sound and Vibration* **81,** 311–335.
Mead, D. J. (1971) Vibration response and wave propagation in periodic structures. *Journal of Engineering for Industry* **93,** 783–792.
Mead, D. J. (1975) Wave propagation and natural modes in periodic systems, I: mono-coupled systems. *Journal of Sound and Vibration* **40,** 1–18.
Mead, D. J. (1975) Wave propagation and natural modes in periodic systems, II: multi-coupled systems with and without damping. *Journal of Sound and Vibration* **40,** 19–39.
Mead, D. J. (1986) A new method of analyzing wave propagation in periodic structures: applications to periodic Timoshenko beams and stiffened plates. *Journal of Sound and Vibration* **104,** 9–27.
Mead, D. J. and Bansal, A. S. (1978) Free wave propagation and response to convected loadings. *Journal of Sound and Vibration* **61,** 481–515.
Mead, D. J. and Lee, S. M. (1984) Receptance methods and the dynamics of disordered one-dimensional lattices. *Journal of Sound and Vibration* **92,** 427–445.
Robinson, C. W. (1972) Shear waves in layered composites. *Report SCL-RR*-720351, Sandia National Laboratories, Albuquerque, U.S.A.
Rousseau, M. (1989) Floquet wave properties in a periodically layered medium. *Journal of the Acoustical Society of America* **86,** 2369–2376.
Rytov, S. M. (1956) Acoustical properties of a thinly laminated medium. *Soviet Physics-Acoustics* **2,** 68–70.
Shah, A. H. and Datta, S. K. (1982) Harmonic waves in a periodically laminated medium. *International Journal of Solids and Structures* **18,** 301–317.
Sun, C. T., Achenbach, J. D. and Herrmann, G. (1968) Time harmonic waves in a stratified medium, propagating in the direction of the layering. *Journal of Applied Mechanics* **35,** 408–411.
Tenenbaum, R. A. and Zindeluk, M. (1992) An exact solution for the one-dimensional elastic wave equation in layered media. *Journal of the Acoustical Society of America* **92,** 3364–3370.
Thomson, W. (1950) Transmission of elastic waves through a stratified medium. *Journal of Applied Physics* **21,** 89–93.
Wang, Y. Y. and Lee, K. H. (1973) Propagation of a disturbance in a chain of interacting harmonic oscillators. *American Journal of Physics* **41,** 51–54.
Whitham, G. B. (1973) *Linear and Nonlinear Waves.* Wiley, New York.

APPENDIX A: MODEL A: FINITE MASS–SPRING CHAIN

As an approximation to the continuum bi-periodic system including m_s hard layers of material A, bonded by (m_s-1) weak layers of material B, consider the following lumped mass–spring system consisting of m_s masses "m_e" connected by (m_s-1) springs with stiffness "k_e".

$$m_e = \rho_A h_A + \rho_B h_B$$
$$k_e = (h_A/E_A + h_B/E_B)^{-1}. \tag{A1}$$

In terms of axial displacement u_i of each mass i, the equations of motion are

$$\ddot{u}_1 + \omega_e^2(u_1 - u_2) = F(t)/m_e$$
$$\ddot{u}_i + \omega_e^2(2u_i - u_{i-1} - u_{i+1}) = 0; \quad 2 \leqslant i \leqslant (m_s - 1)$$

$$\ddot{u}_{m_s}+\omega_e^2(u_{m_s}-u_{m_{s-1}})=0 \tag{A2}$$

where $(\dot{})$ is the time derivative and ω_e is the frequency of the set

$$\omega_e=(k_e/m_e)^{1/2}=\left[\frac{E_B}{\rho_A h_A h_B(1+\tilde{z}^{-1})[1+(\tilde{z}\tilde{\tau})^{-1}]}\right]^{1/2}=\frac{1}{2}\Delta\omega_{PZ1} \tag{A3}$$

where $\Delta\omega_{PZ1}$ is the frequency width of PZ1. The eigenstates are determined by solving

$$\det[\mathbf{K}-\omega^2\mathbf{I}]=0$$

$$\mathbf{K}=\omega_e^2\begin{bmatrix}1&-1&0&0&\dots&0&0\\-1&2&-1&0&\dots&0&0\\0&-1&2&-1&\dots&0&0\\\vdots&\vdots&\vdots&\vdots&\vdots&\vdots&\vdots\\0&0&0&0&\dots&-1&1\end{bmatrix} \tag{A4}$$

where $\mathbf{I}$ is the unit matrix. By expanding in eigenfunctions

$$\mathbf{u}=\sum_j a_j(t)\Phi_j \tag{A5}$$

in (A2) and by orthogonality of Φ_j a solution for $a_j(t)$ in terms of Duhamel's integral results:

$$a_j(t)=\frac{1}{\omega_j N_j}\int_0^t \Phi_{j1}^T F(\tau)\sin\omega_j(t-\tau)\,d\tau$$

$$N_j=m_e\Phi_j^T\mathbf{I}\Phi_j \tag{A6}$$

where Φ_{j1} is the first component of the eigenvector Φ_j.

If the system (A2) were infinite in extent, a Floquet solution periodic in time and space would take the form:

$$u_{i+1}=e^{\mu}u_i. \tag{A7}$$

Substituting (A7) in (A2) with $\ddot{u}_i$ replaced by $-\omega^2 u_i$ yields

$$-\omega^2+2\omega_e^2(1-\cos\mu)=0\Rightarrow\frac{\mu}{2}=\sin^{-1}\left(\frac{\omega}{2\omega_e}\right). \tag{A8}$$

The propagation constraint μ is related to wave number k by $\mu=kh_s$. Expressions for phase and group velocities c_p and c_g have the form:

$$c_p=\frac{\omega}{k}=c_0\frac{\sin\left(\frac{\mu}{2}\right)}{\frac{\mu}{2}}$$

$$c_g=\frac{\partial\omega}{\partial k}=c_0\cos\left(\frac{\mu}{2}\right)$$

$$c_0=\omega_e h_s. \tag{A9}$$

As $\mu\to 0$, c_p and c_g approach c_0. When $\omega=\omega_e$, $\mu/2=\pi/6$ and by (A9) $c_p=(3/\pi)c_0$ and $c_g=\sqrt{3}/2c_0$. Also, when $\omega=2\omega_e\simeq\Delta\omega_{PZ1}$, $c_p=2/\pi c_0$ and $c_g=0$. In (A9), c_p is velocity of the wave front and c_g is velocity of peak stress σ_{mx}^1. Expressing c_p and c_g in terms of $\tilde{\omega}=\omega/(2\omega_e)$ yields:

$$c_p/c_0=\tilde{\omega}/\sin^{-1}(\tilde{\omega})$$

$$c_g/c_0=\cos[\sin^{-1}(\tilde{\omega})]=(1-\tilde{\omega}^2)^{1/2}. \tag{A10}$$

Both c_p and c_g peak at $\tilde{\omega}=0$ and decrease uniformly with $\tilde{\omega}$.

Stress in the ith spring σ_i is given by

$$\sigma_i=k_e(u_i-u_{i-1}). \tag{A11}$$

Substituting (A11) in (A2) yields the relations

$$m_e\ddot{u}_1 + \sigma_1 = F(t)$$
$$m_e\ddot{u}_i + \sigma_i = \sigma_{i-1}; \quad 2 \leqslant i \leqslant m_s. \tag{A12}$$

Integrating (A12) gives

$$m_e\dot{u}_1|_0^{t_L} + \int_0^{t_L} \sigma_1 \, dt = \int_0^{t_L} F(t) \, dt \equiv I_p$$
$$m_e\dot{u}_i|_0^{t_L} + \int_0^{t_L} \sigma_i \, dt = \int_0^{t_L} \sigma_{i-1} \, dt \tag{A13}$$

where I_p is the external impulse. Figure (1a) reveals that after the passage of the wave front, a motionless plateau develops in u prior to reflections from the boundary. If t_L is sufficiently large to lie in the motionless plateau, the first term becomes negligible and (A13) expresses conservation of momentum:

$$\int_0^{t_L} \sigma_1 \, dt = \mathbf{I}_p$$
$$\int_0^{t_L} \sigma_i \, dt = \int_0^{t_L} \sigma_{i-1} \, dt = \mathbf{I}_p. \tag{A14}$$

For a rectangular forcing pulse of unit intensity applied to a semi-infinite periodic chain, an analytical expression for transient stress response can be derived by inverting the Fourier transform integral. Transforming the dynamic eqns (A2) yields

$$-4\tilde{\omega}^2\bar{u}_0 + (\bar{u}_0 - \bar{u}_1) = \frac{\bar{\sigma}_0}{m_e\omega_e^2}; \quad n = 0 \tag{A15a}$$

$$-4\tilde{\omega}^2\bar{u}_n + (2\bar{u}_n - \bar{u}_{n-1} - \bar{u}_{n+1}) = 0; \quad n \geqslant 1 \quad \bar{u}_n(\omega) = \frac{1}{\sqrt{2\pi}}\int_{-\infty}^{\infty} u_n(t)\, e^{i\omega t} \, dt \tag{A15b}$$

where $\sigma_0 = 1$ is magnitude of the forcing pulse and $\bar{\sigma}_0$ is its transform. Periodicity requires that

$$\bar{u}_n = e^{\mu}\bar{u}_{n-1} \tag{A16}$$

where μ is propagation constant. Substituting (A16) in (A15b) yields the dispersion relation

$$e^{\mu} = 1 - 2\tilde{\omega}^2 + 2\tilde{\omega}(\tilde{\omega}^2 - 1)^{1/2}. \tag{A17}$$

Substituting (A16) in (A15a) and eliminating e^{μ} using (A17) gives the transformed impedance at the excited end

$$\bar{u}_0 = \frac{\bar{\sigma}_0}{m_e\omega_e^2} \frac{1}{2[\tilde{\omega}^2 + \tilde{\omega}(\tilde{\omega}^2 - 1)^{1/2}]}. \tag{A18}$$

Expressing $\bar{u}_n$ in terms of $\bar{u}_0$ by repeated use of (A16) gives

$$\bar{u}_n = [1 - 2\tilde{\omega}^2 + 2\tilde{\omega}(\tilde{\omega}^2 - 1)^{1/2}]^n\bar{u}_0. \tag{A19}$$

The inverse Fourier transform of (A19) is:

$$u_n(t) = \frac{1}{\sqrt{2\pi}}\int_{-\infty}^{\infty} [1 - 2\tilde{\omega}^2 + 2\tilde{\omega}(\tilde{\omega}^2 - 1)^{1/2}]^n\bar{u}_0(\omega)\, e^{-i\omega t} \, d\omega. \tag{A20}$$

Following Wang and Lee (1973) which specializes in outgoing waves, the integral in (A20) simplifies to:

$$u_n(t) = \delta_{n0}u_0(t) + 2n\int_0^t \frac{J_{2n}[2\omega_e(t-t')]}{(t-t')} u_0(t') \, dt' \tag{A21}$$

where J is the Bessel function of the first kind. Equation (A21) applies also to normalized stress in the form:

$$\sigma_n(t) = \delta_{n0} + 2n\int_0^t \frac{J_{2n}[2\omega_e(t-t')]}{(t-t')} \, dt'. \tag{A22}$$

Equation (A22) is the convolution integral of stress transmissibility at the nth interface. Re-writing the integral in (A22) as

$$\int_0^t \frac{J_{2n}[\beta(t-t')]}{t-t'}\,dt' = -\int_0^t \frac{J_{2n}(\beta\tau)}{\tau^{2n-1}}\tau^{2n-2}\,d\tau; \quad \beta = 2\omega_e$$

then integrating by parts noting that (see Gradshteyn and Ryzhik, 1970)

$$\int^t \frac{J_m(\beta\tau)}{\tau^{m-1}}d\tau = -\frac{J_{m-1}(\beta t)}{\beta t^{m-1}}$$

yields an exact expression for stress transmissibility when $t \leqslant t_f$, where t_f is the time interval of the forcing pulse

$$\sigma_n(t) = 1 - \sum_{k=0}^{n-1} \frac{2^{n-k}n!}{k!}\frac{J_{n+k}(\beta t)}{(\beta t)^{n-k}}; \quad t \leqslant t_f. \tag{A23}$$

For $t > t_f$, changing the upper limit of (A21) to t_f noting that

$$\int_0^t F(t-t')\,dt' = \int_{t_f}^{\hat{t}} F(\tau)\,d\tau; \quad \hat{t} = t - t_f$$

then following the procedure that led to (A23) yields

$$\sigma_n(t) = \sum_{k=0}^{n-1} \frac{2^{n-k}n!}{k!}\left[\frac{J_{n+k}(\beta\hat{t})}{(\beta\hat{t})^{n-k}} - \frac{J_{n+k}(\beta t)}{(\beta t)^{n-k}}\right]; \quad t > t_f. \tag{A24}$$

In PZ1, $\sigma_n(t)$ along the nth layer varies linearly (see eqns (6) and (7))

$$\sigma_{n,n+1}(\xi, t) = (1-\xi)\sigma_n(t) + \xi\sigma_{n+1}(t) \tag{A25}$$

where $\xi = x/h_A$ is the normalized local axial coordinate along the hard layer of the nth periodic set. Equation (A24) shows that for large t, $\sigma_n(t)$ is periodic with frequency $\beta = 2\omega_e \simeq \Delta\omega_{PZ1}$. Displacement follows from eqn (16b) of Wang and Lee (1973):

$$\begin{aligned} u_0(t) &= \frac{1}{m_e\omega_0}\int_{-\infty}^{t}\int_0^{t-t'} \frac{J_1(\beta t'')}{t''}\,dt'' \\ &= \frac{1}{m_e\omega_0}\int_{-\infty}^{t}\left\{J_1[\beta(t-t')] + 2\sum_{k=1}^{\infty} J_{2k+1}[\beta(t-t')]\right\}dt'. \end{aligned} \tag{A26}$$

Displacement at other junctions then follows from

$$u_n(t) = u_{n-1}(t) - \sigma_n(t)/k_e. \tag{A27}$$

APPENDIX B: MODEL B: OSCILLATOR WITH DELAYED MOVING BASE

Figure 10(a) illustrates the oscillator with moving base. The mass m_e with displacement $u(t)$ is driven by $F(t)$ against a spring with stiffness k_e attached to a moving base with displacement $u(t-t_d)$. It is assumed that $u(t) = 0$ when $t < 0$. The moving base model assumes

$$\begin{aligned} u_2(t) &= u_1(t-t_{d1}) \\ u_{i+1}(t) &= u_i(t-t_{di}), \quad i > 1 \\ t_{d1} &= c_p(\omega_e)/h_s = \frac{3}{\pi}c_0/h_s; \quad t_{di} = c_0. \end{aligned} \tag{B1}$$

Substituting (B1) in (A2) produces

$$\begin{aligned} \ddot{u}_1(t) + \omega_e^2[u_1(t) - u_1(t-t_d)] &= F(t)/m_e \\ \ddot{u}_1(t) + \omega_e^2[u_1(t) - u_1(t-t_d)] &= \sigma_{i-1}(t)/m_e \\ \sigma_{i-1}(t) &= k_e[u_{i-1}(t) - u_{i-1}(t-t_d)] \end{aligned} \tag{B2}$$

where $F(t) = \sigma_0[H(t) - H(t-t_f)]$ and ω_e, m_e, c_p are frequency, mass and phase velocity of Model A.

A solution to eqn (B2) proceeds by segmenting time into intervals of width t_d. In the first interval $0 \leqslant t \leqslant t_d$, $u(t-t_d) = 0$ and $u_1(t)$ is easily found. In each succeeding interval, $u(t-t_d)$ is the u determined in the prior interval,

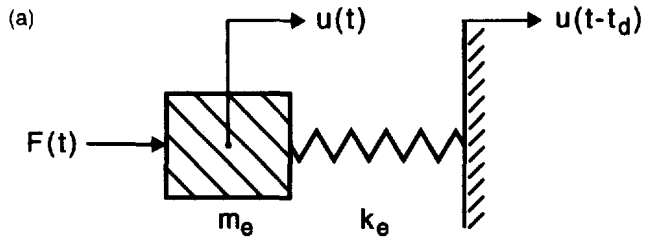

Fig. 10(a). Oscillator with moving base.

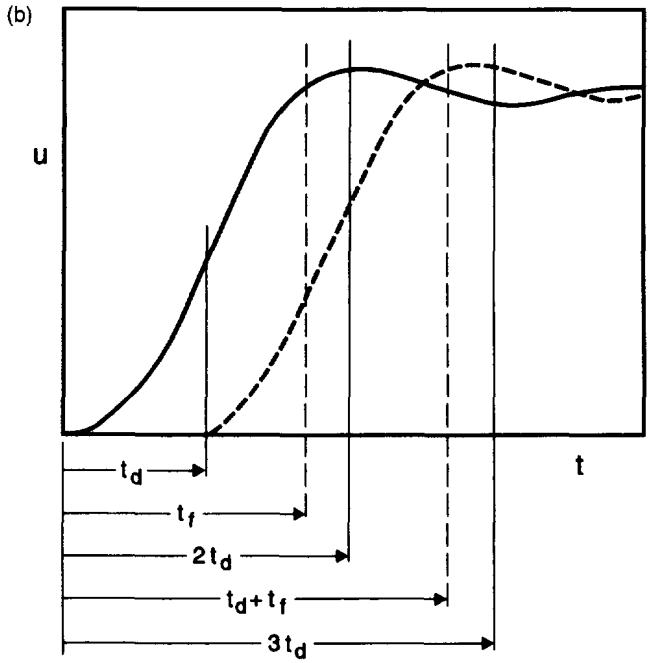

Fig. 10(b). Time segments in moving base model.

making the forcing function known. This simple recursion becomes slightly more complex during the Jth interval $Jt_d \leqslant t_f \leqslant (J+1)t_d$. This and all subsequent intervals are further segmented into two subintervals:

$$Jt_d \leqslant t \leqslant t_f; \quad t_f \leqslant t \leqslant (J+1)t_d$$
$$(J+1)t_d \leqslant t \leqslant t_d+t_f; \quad t_d+t_f \leqslant t \leqslant (J+2)t_d \tag{B3}$$

as shown schematically in Fig. 10(b).

Three special cases arise when t_f lies in the first, second or third t_d interval. Now specializing to the first layer a new notation is used; subscripts refer to mass number, as in (B1) and (B2), but to time interval and sub-interval numbers. When $t \leqslant Jt_d$, a single subscript is used denoting interval number. When $t > Jt_d$, a double subscript is used; the first denotes interval number while the second denotes sub-interval number. For the case when $0 \leqslant t_f \leqslant t_d$, the process yields

$(1)_1$ $0 \leqslant t \leqslant t_f$

$$u_{11}(t) = \frac{1}{\omega_e}\int_0^t \frac{\sigma_0}{m_e}\sin\omega_e(t-\tau)\,d\tau = \frac{\sigma_0}{k_e}(1-\cos\omega_e t)$$
$$\sigma_{11}(t) = k_e u_{11}(t) \tag{B4a}$$

$(1)_2$ $t_f \leqslant t \leqslant t_d$

$$u_{12}(t) = u_{11}(t_f)\cos\omega_e(t-t_f) + \frac{\dot{u}_{11}(t_f)}{\omega_e}\sin\omega_e(t-t_f)$$
$$= \frac{\sigma_0}{k_e}[-\cos\omega_e t + \cos\omega_e(t-t_f)]$$
$$\sigma_{12}(t) = k_e u_{12}(t) \tag{B4b}$$

$(2)_1$ $t_d \leqslant t \leqslant t_d + t_f$

$$u_{21}(t) = u_{12}(t_d)\cos\omega_e(t-t_d) + \frac{\dot{u}_{12}(t_d)}{\omega_e}\sin\omega_e(t-t_d) + \omega_e\int_{t_d}^{t} u_{11}(\tau-t_d)\sin\omega_e(t-\tau)\,d\tau$$

$$u_{21}(t) = \frac{\sigma_0}{k_e}\left[1-\cos\omega_e t-\cos\omega_e(t-t_d)+\cos\omega_e(t-t_f)-\frac{\omega_e}{2}(t-t_d)\sin\omega_e(t-t_d)\right]$$

$$\sigma_{21}(t) = k_e[u_{21}(t)-u_{11}(t-t_d)]$$

$$= \sigma_0\left[-\cos\omega_e t+\cos\omega_e(t-t_f)-\frac{\omega_e}{2}(t-t_d)\sin\omega_e(t-t_d)\right]. \tag{B4c}$$

A similar process applies to the cases when $t_d \leqslant t_f \leqslant 2t_d$ and $2t_d \leqslant t_f \leqslant 3t_d$, etc.

The second step in building Model B develops an expression for the attenuating of σ^1_{mx} in layers below the first. In Whitham (1973), wave amplitude $A(x, t_p)$ is related to arrival time t_p asymptotically in a uniaxial dispersive medium. $A(x, t)$ is expressed as a Fourier integral.

$$A(x,t) = \int_{-\infty}^{\infty} F(\kappa)\exp[i\kappa x - iW(\kappa)t]\,d\kappa \tag{B5}$$

where $F(\kappa)$ is an arbitrary function satisfying initial and boundary conditions, and $\omega = W(k)$ is the dispersion relation. To find the asymptotic expression for large x and t provided (x/t) is held fixed, re-write (B5) as

$$A(x,t) = \int_{-\infty}^{\infty} F(\kappa)\,e^{-i\chi t}\,d\kappa$$

$$\chi(\kappa) = W(\kappa) - \kappa\frac{x}{t}; \quad \frac{x}{t}\text{ fixed.} \tag{B6}$$

By the method of steepest descent, the main contribution to the integral in (B6) is from the neighborhood of stationary point $\kappa = k$ such that

$$\chi'(k) = W'(k) - \frac{x}{t} = 0. \tag{B7}$$

If $\chi''(k) \neq 0$, it will be assumed that $F(\kappa)$, $\chi(\kappa)$ can be expanded in Taylor series near $\kappa = k$

$$F(\kappa) \simeq F(k)$$

$$\chi(\kappa) \simeq \chi(k) + \tfrac{1}{2}(\kappa-k)^2\chi''(k). \tag{B8a}$$

Substituting (B8A) in (B6) and invoking the error integral yields

$$A(x,t_p) \simeq \sum_{\text{S.P.}} F(k)\left[\frac{2\pi}{t_p|W''(k)|}\right]^{1/2}\exp\left[ikx - iW(k)t_p - \frac{i\pi}{2}\operatorname{sgn} W''(k)\right] \tag{B8b}$$

where the sum is over all stationary points k. If $\chi''(k) = 0$ and $\chi'''(k) \neq 0$, then the expansion for $\chi(\kappa)$ becomes

$$\chi(\kappa) \simeq \chi(k) + \tfrac{1}{6}(\kappa-k)^3\chi'''(k) \tag{B9a}$$

producing the asymptotic amplitude

$$A(x,t_p) \simeq \left(\frac{1}{3}\right)!\,2^{1/3}3^{5/6}\sum_{\text{s.p.}}\frac{F(k)}{[t_p|W'''(k)|]^{1/3}}\exp[ikx - iW(k)t_p]. \tag{B9b}$$

For the present case, $W(k)$ is given implicitly by eqn (12). Specializing in waves in PZ1, reduces (12) to (A8), which when inverted yields the form

$$W(k) = \frac{2}{h_s}c_0\sin\left(\frac{1}{2}kh_s\right) \tag{B10a}$$

with derivatives

$$W'(k) = c_0\cos(\tfrac{1}{2}kh_s) \tag{B10b}$$

$$W''(k) = -\tfrac{1}{2}c_0h_s\sin(\tfrac{1}{2}kh_s) \tag{B10c}$$

$$W'''(k) = -\tfrac{1}{4}c_0h_s^2\cos(\tfrac{1}{2}kh_s). \tag{B10d}$$

From (B10b), $k_n = 4n\pi/h_s$ is a stationary point because

$$W'(k_n) - \frac{x}{t} \equiv W'(0) - c_0 = 0.$$

Since $W''(k_n) = 0$ and $W'''(k_n) \neq 0$, the asymptotic behavior emerges from (B9b)

$$\sigma^1_{mx}(x, t_p) \propto t_p^{-1/3}. \tag{B11}$$

More generally, at any point in the stack σ^1_{mx}, can be expected to obey

$$\sigma^1_{mx} \propto t_p^{-\alpha} \tag{B12}$$

where the attenuation index α is determined numerically.

APPENDIX C: MODEL C: TRANSMISSION OF ELASTIC FREQUENCIES OF THE HARD LAYER

If we consider that the first hard layer is acted upon its left by the trapezoidal pulse $F_L(t)$ and on its right by the reaction of the soft layer $F_R(t)$:

$$F_L(t) = \frac{t}{t_1}\sigma_0[H(t) - H(t_1)] + \sigma_0[H(t-t_1) - H(t-t_2)] + \sigma_0\left[-\frac{(t-t_2)}{(t_3-t_2)} + 1\right][H(t-t_2) - H(t-t_3)] \tag{C1}$$

$$F_R(t) \simeq \frac{\eta\sigma_0}{2}\left(1 - \cos\frac{2\pi t}{T}\right) \tag{C2}$$

where $\eta < 1$. Equation (C2) is the same as (1) with σ^1_{mx} replaced by $\eta\sigma_0$. From the definition of t_f

$$t_f = \tfrac{1}{2}(t_1 + t_2 + t_3) - t_1 \tag{C3}$$

and from (A17) for $2t_f < \pi/\omega_e$

$$T = \pi/\omega_e = \pi h_s/c_0. \tag{C4}$$

If $u(x, t)$ is expressed as the superposition of static and dynamic solutions to each of $F_L(t)$ and $F_R(t)$

$$u(x, t) = u_{dL}(x, t) + u_{sL}(x)F_L(t) + u_{dR}(x, t) + u_{sR}(x)F_R(t) \tag{C5}$$

where subscripts s and d denote static and dynamic solutions. If $u_{dL}(x, t)$ is expanded in eigenfunctions of the traction-free layer

$$u_{dL}(x, t) = \sum_i a_{iL}(t)\varphi_i(x)$$

$$\ddot{a}_{iL} + \omega_i^2 a_{iL} = -\frac{1}{N_i}\left[\rho_A\langle u_{sL} \mid \varphi_i\rangle\ddot{F} + \frac{1}{h_A}\langle\varphi_i \mid 1\rangle F\right]$$

$$N_i = \rho_A\langle\varphi_i \mid \varphi_i\rangle \tag{C6}$$

and similarly for $u_{dR}(x, t)$. For the fundamental mode of the hard layer

$$\varphi_1(x) = \cos(\pi x/h_A), \quad \omega_1 = \pi c_A/h_A \tag{C7}$$

the static solutions are

$$u_{sL}(x) = \frac{h_A}{E_A}\left(\xi - \frac{1}{2}\xi^2 - \frac{1}{3}\right)$$

$$u_{sR}(x) = \frac{h_A}{E_A}\left(\frac{1}{2}\xi^2 - \frac{1}{6}\right); \quad \xi = \frac{x}{h_A}. \tag{C8}$$

Using (C7) and (C8) in (C6) yields

$$N_a \equiv \langle\varphi_1 \mid 1\rangle = 0; \quad N_1 = \tfrac{1}{2}\rho_A h_A$$

$$N_{sL} \equiv \langle u_{sL} \mid \varphi_1\rangle = h_A/\pi^2$$

$$N_{sR} \equiv \langle u_{sR} \mid \varphi_1\rangle = h_A/\pi^2. \tag{C9}$$

Solving and summing contributions from $a_{1L}(t)$ and $a_{1R}(t)$ yields:

(A) $0 \leqslant t \leqslant t_1$

$$u_d(x,t) = -\sigma_0 \frac{h_A}{E_A}\frac{2}{\pi^2}\frac{\sin\omega_1 t}{\omega_1 t_1}\cos\pi\xi$$

$$-\sigma_0 \frac{h_A}{E_A}\eta\frac{4}{T^2}\frac{\left(\cos\frac{2\pi t}{T}-\cos\omega_1 t\right)}{(\omega_1^2-4\pi^2/T^2)}\cos\pi\xi$$

$$u_s(x)F(t) = \sigma_0\frac{h_A}{E_A}\left[\frac{t}{t_1}\left(\xi-\frac{1}{2}\xi^2-\frac{1}{3}\right)+\frac{\eta}{2}\left(1-\cos\frac{2\pi t}{T}\right)\left(\frac{1}{2}\xi^2-\frac{1}{6}\right)\right]$$

$$\sigma_d(x,t) = \sigma_0\left\{\frac{2}{\pi}\frac{\sin\omega_1 t}{\omega_1 t_1}+\eta\frac{4\pi}{T^2}\frac{\left(\cos\frac{2\pi t}{T}-\cos\omega_1 t\right)}{(\omega_1^2-4\pi^2/T^2)}\right\}\sin\pi\xi$$

$$\sigma_s(x)F(t) = \sigma_0\left\{\frac{t}{t_1}(1-\xi)+\frac{\eta}{2}\left(1-\cos\frac{2\pi t}{T}\right)\xi\right\}. \tag{C10}$$

If $2\omega_e < \omega_1$

$$\sigma_{dL} \leqslant \frac{2}{\pi}\frac{\sigma_0}{\omega_1 t_1}, \quad \sigma_{dR} \leqslant \frac{2}{\pi}\eta\sigma_0\left(\frac{2\omega_e}{\omega_1}\right)^2 \Rightarrow \sigma_{dR} < \eta\omega_1 t_1\left(\frac{2\omega_e}{\omega_1}\right)^2\sigma_{dL} \tag{C11}$$

from which $\sigma_{dR}(t)$ may be neglected.

(B) $t_1 \leqslant t \leqslant t_2$

$$u_d(x,t) \simeq -\sigma_0\frac{2}{\pi^2}\frac{h_A}{E_A}\frac{1}{\omega_1 t_1}[\sin\omega_1 t-\sin\omega_1(t-t_1)]\cos\pi\xi$$

$$u_s(x)F(t) = \sigma_0\frac{h_A}{E_A}\left[\left(\xi-\frac{1}{2}\xi^2-\frac{1}{3}\right)+\frac{\eta}{2}\left(1-\cos\frac{2\pi t}{T}\right)\left(\frac{1}{2}\xi^2-\frac{1}{6}\right)\right]$$

$$\sigma_d(x,t) \simeq \sigma_0\frac{2}{\pi}\frac{1}{\omega_1\omega_1}[\sin\omega_1 t-\sin\omega_1(t-t_1)]\sin\pi\xi$$

$$\sigma_s(x)F(t) = \sigma_0\left[1-\xi+\frac{\eta}{2}\left(1-\cos\frac{2\pi t}{T}\right)\xi\right]. \tag{C12}$$

To first order, σ_d vanishes if

$$[\sin\omega_1 t-\sin\omega_1(t-t_1)] = 0. \tag{C13}$$

(C13) is satisfied for all t if

$$\omega_1 t_1 = 2j\pi \Rightarrow t_1 = \frac{2j\pi}{\omega_1} \equiv \frac{j}{\Omega_1}. \tag{C14}$$

Since $\omega_i = i\omega_1$, elastic waves of the hard layer are not transmitted when the product of fundamental frequency ω_1 and rise time t_1 is a multiple of 2π.